

Structure and Catalytic Properties of Supported Vanadium Oxides: Support Effects on Oxidative Dehydrogenation Reactions

Andrei Khodakov, Bryan Olthof, Alexis T. Bell,¹ and Enrique Iglesia¹

Chemical Sciences Division and Materials Sciences Division, E.O. Lawrence Berkeley National Laboratory, and Department of Chemical Engineering, University of California at Berkeley, Berkeley, California 94720-1462

E-mail: {iglesia, bell}@cchem.berkeley.edu

Received April 30, 1998; revised August 21, 1998; accepted October 7, 1998

The effects of support (Al_2O_3 , SiO_2 , HfO_2 , TiO_2 , and ZrO_2) on the structure and catalytic behavior of supported vanadia in the oxidative dehydrogenation of propane were examined over a wide range of vanadium surface densities ($0.5\text{--}15.0 \text{ VO}_x/\text{nm}^2$). X-ray diffraction and Raman and UV-visible spectra showed that vanadia exists as highly dispersed species at surface densities below $7 \text{ VO}_x/\text{nm}^2$ on Al_2O_3 , HfO_2 , TiO_2 , and ZrO_2 , but as large V_2O_5 crystallites on SiO_2 . Surface structures evolve from isolated monovanadates to polyvanadate domains and V_2O_5 crystallites as VO_x surface density increases. Polyvanadates appear at lower surface densities on ZrO_2 and TiO_2 than on Al_2O_3 and HfO_2 . UV-visible edge energies decrease as VO_x domains grow with increasing VO_x surface density on all supports. Initial propene selectivities increase with increasing VO_x surface density, as monovanadate species and exposed support sites, which favor primary combustion pathways, decrease in concentration. Oxidative dehydrogenation rates per V-atom reach a maximum on VO_x domains of intermediate size, which provide a balance between the activity of surface VO_x species and their accessibility to reactants. Interactions with supports determine the type of VO_x structures present at a given surface density, but turnover rates do not depend on the identity of the support when differences in VO_x structure are taken into account. Oxidative dehydrogenation turnover rates are similar on polyvanadate species and on surface VO_x sites on bulk V_2O_5 . The relative rates of oxidative dehydrogenation to form propene and of secondary propene oxidation to CO_x do not depend on the identity of the support or on VO_x surface density or structure. Thus, it appears that these two reactions require similar VO_x surface sites and that these sites are present at similar surface densities on polyvanadate domains and small V_2O_5 clusters. © 1999 Academic Press

INTRODUCTION

Oxidative dehydrogenation of alkanes provides a thermodynamically accessible route to the synthesis of alkenes from alkanes (1–3). Supported vanadium oxides (VO_x) catalyze this reaction, but unselective combustion pathways

limit alkene selectivities, especially at high conversions (4–18). The local coordination and symmetry of V^{+5} centers in bulk and supported V_2O_5 have been frequently implicated in the observed effects of support, VO_x concentration, and pretreatment procedures on catalytic behavior. Many of these structure–function relations remain incomplete because of difficult structural characterization, undetected transport restrictions, and kinetic analyses complicated by parallel and sequential combustion pathways.

The extent of dispersion and the local and extended structure of supported VO_x species depend on the chemical identity and the surface area of the support (1–3, 17, 18). Previous studies have shown that basic metal oxides (e.g., MgO , Bi_2O_3 , La_2O_3 , Sm_2O_3) lead to supported VO_x species with higher alkene selectivities than when acidic oxides are used as supports (1, 13–15). Several authors have proposed that acidic V_2O_5 species interact weakly with acidic supports, leading to poorly dispersed V_2O_5 crystallites (13, 15).

The structure of selective VO_x species and the reaction pathways in oxidative dehydrogenation of alkanes remain subjects of active discussion. Our recent study (4) combined spectroscopic and chemical characterization methods with detailed kinetic analyses of oxidative dehydrogenation pathways in order to address these issues on VO_x/ZrO_2 catalysts. This work showed that the structure and catalytic behavior of these materials depend strongly on VO_x surface density. Polyvanadate species that form on ZrO_2 at VO_x surface densities above $3\text{--}4 \text{ VO}_x/\text{nm}^2$ provide active and selective sites for oxidative dehydrogenation reactions. Catalysts with lower VO_x surface density and uncovered ZrO_2 surfaces show lower alkene selectivities because of competing oxidation pathways leading to undesired CO and CO_2 products.

In this study, we examine the effect of support (Al_2O_3 , SiO_2 , HfO_2 , TiO_2 , and ZrO_2) on the structure and catalytic behavior of VO_x species over a wide range of VO_x surface densities. X-ray diffraction, Raman spectroscopy, and UV-visible spectroscopy were used to examine the structure and electronic properties of supported VO_x species. Rate

¹ To whom correspondence should be addressed.

constants for primary and secondary reaction pathways were obtained by kinetic analysis of steady-state oxidative dehydrogenation rates obtained in differential flow reactors.

EXPERIMENTAL

TiO₂ (Süd-Chemie, AG), Al₂O₃ (Degussa, AG), and SiO₂ (Davison Chemical) supports were obtained from commercial sources. Zirconium (ZrO(OH)₂) and hafnium (HfO(OH)₂) oxyhydroxides were prepared from the corresponding oxychlorides by coprecipitation at controlled pH (4). Vanadium was introduced at various concentrations (Table 1) via incipient wetness impregnation of supports with aqueous ammonium metavanadate solutions (99%, Aldrich, Inc.) (4, 21). These solutions also contained oxalic acid (Mallinckrodt, analytical grade; NH₄VO₃/oxalic acid = 0.5 M) in order to ensure dissolution of ammonium metavanadate precursors. After impregnation, samples were dried overnight in air at 393 K and treated in dry air at 773 K for 3 h.

Surface areas were measured in a N₂ physisorption flow apparatus using thermal conductivity detection and multi-point BET analysis methods. Samples were dehydrated in He at 473 K for 1 h before surface area measurements. Powder X-ray diffraction patterns were obtained at room

temperature using Cu (K_α) radiation and a Siemens D5000 diffractometer. A small amount of catalyst was mixed with vaseline, spread smoothly onto a thin glass plate, and placed in the diffractometer.

Raman spectra were obtained using a HoloLab 5000 Raman research spectrophotometer (Kaiser Optical Systems, Inc). Samples (0.1 g) were pressed at 70 MPa pressure into wafers (0.9 cm diameter, 0.1 cm thickness) and mounted in a quartz cell. This cell can be heated up to 1073 K and gases can be introduced for *in situ* measurements during treatments. Raman spectra were recorded in the 100 to 1300 cm⁻¹ wavenumber range using a 532-nm laser line.

Diffuse reflectance UV-visible spectra were obtained using MgO as a reference in a Varian-Cary 4 spectrophotometer equipped with a Harrick diffuse-reflectance attachment. Reflectance data were converted to absorption spectra using Kubelka–Munk functions (22). The sample cell was equipped with a heater unit, a water cooling system, a thermocouple, and a gas flow system for *in situ* measurements. UV-visible electronic spectra of samples dehydrated *in situ* in dry air at 723 K for 30 min were measured in the 1.5–6.0 eV energy range at room temperature.

Oxidative dehydrogenation rates and selectivities were measured in a fixed-bed quartz reactor using catalyst samples (0.015–0.3 g) diluted with quartz powder (0.5 g) in order to prevent temperature gradients. A mixture of C₃H₈ (14.0 kPa) and O₂ (1.74 kPa) in He was introduced into the reactor at controlled flow rates. Reactant and product concentrations were measured by gas chromatography (Hewlett-Packard 5880 GC, Carboxen packed column, thermal conductivity detection). Only C₃H₆, H₂O, CO, and CO₂ were detected as reaction products. Larger product samples injected into a capillary column also failed to detect any other reaction products. Bed residence times and C₃H₈ and O₂ conversions were varied by changing the feed flow rate between 0.5 and 6 cm³(STP) s⁻¹. C₃H₈ and O₂ conversions were below 1% and 20%, respectively. The rates of formation of propene, CO, and CO₂ were extrapolated to zero conversion in order to estimate the rates of primary C₃H₈ dehydrogenation and oxidation steps. Rate constants for primary and secondary steps were obtained using a previously reported kinetic analysis method (4).

RESULTS

Catalyst surface areas and calculated VO_x surface densities (*n_s*) are shown in Figs. 1a and 1b and in Table 1 as a function of V₂O₅ content for Al₂O₃, SiO₂, HfO₂, TiO₂, and ZrO₂ supports after treatment in air at 773 K for 3 h. Each catalyst is identified as, for example, 0.7 VO_x/Al₂O₃, where 0.7 defines the weight loading of vanadia as V₂O₅. The presence of VO_x had only a modest effect on the surface area of the support (Fig. 1a). As a result, VO_x surface densities increased almost linearly with increasing V₂O₅ content

TABLE 1

Vanadium Content, Surface Area, and Calculated VO_x Surface Density for Supported Vanadium Oxide Catalysts Studied

Support	Catalyst	V ₂ O ₅ content (wt%)	BET surface area (<i>S</i> _{BET}) m ² /g	VO _x surface density, nm ⁻² (<i>n_s</i>)
Al ₂ O ₃	0.7VO _x /Al ₂ O ₃	0.7	88	0.5
	2VO _x /Al ₂ O ₃	2	100	1.3
	3.5VO _x /Al ₂ O ₃	3.5	100	2.3
	5VO _x /Al ₂ O ₃	5	96	3.5
	10VO _x /Al ₂ O ₃	10	86	7.7
	15VO _x /Al ₂ O ₃	15	89	11.1
SiO ₂	2VO _x /SiO ₂	2	287	0.46
	5VO _x /SiO ₂	5	283	1.2
	10VO _x /SiO ₂	10	271	2.4
	15VO _x /SiO ₂	15	251	4.0
TiO ₂	0.7VO _x /TiO ₂	0.7	73.5	0.63
	2VO _x /TiO ₂	2	69.0	1.9
	3.5VO _x /TiO ₂	3.5	69.5	3.3
	5VO _x /TiO ₂	5	58	5.7
HfO ₂	1.2VO _x /HfO ₂	1.2	62	1.3
	3VO _x /HfO ₂	3	79	2.5
	6.1VO _x /HfO ₂	6.1	125	3.2
	9.4VO _x /HfO ₂	9.4	115	5.4
ZrO ₂	2VO _x /ZrO ₂	2	144	0.92
	5VO _x /ZrO ₂	5	155	2.1
	10VO _x /ZrO ₂	10	170	3.9
	15VO _x /ZrO ₂	15	160	6.2

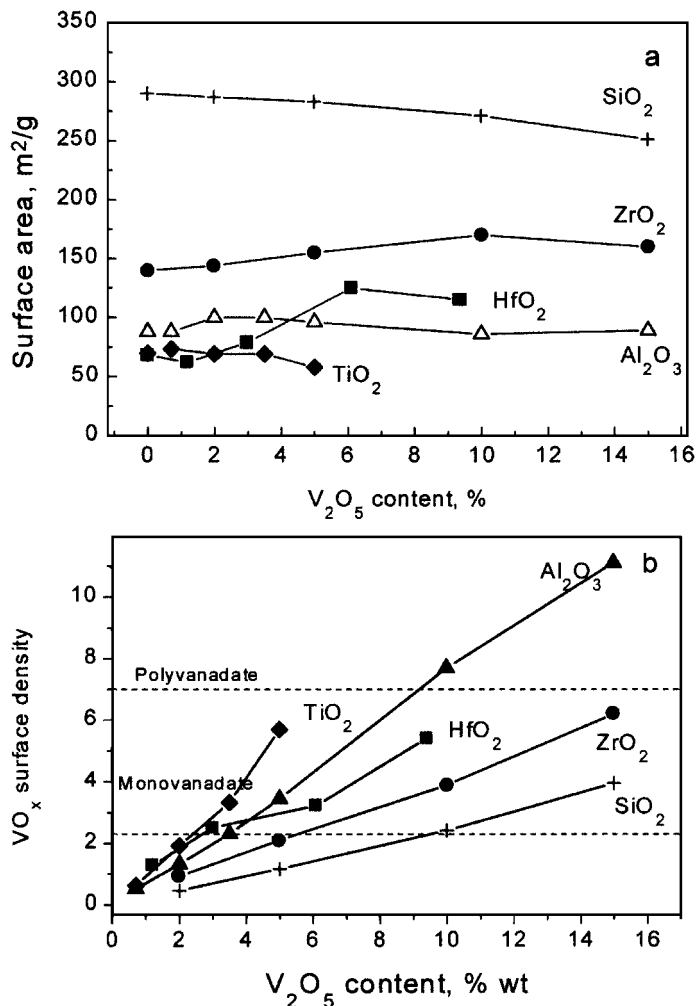


FIG. 1. BET surface areas (a) and VO_x surface densities (b) for supported vanadium oxide catalysts after oxidation treatment at 773 K for 3 h.

(Fig. 1b). The surface density is defined as the number of vanadium atoms per square nanometer of the catalyst and was calculated from the V₂O₅ content and the BET surface area; it provides a convenient parameter for comparing catalysts prepared on supports with a wide range of surface areas. Clearly, at a given vanadium surface density the structure of VO_x species will depend on the ability of a given support to disperse the VO_x species placed on its surface. The dashed lines in Fig. 1b identify VO_x surface densities corresponding to theoretical monovanadate (2.3 VO_x/nm²) or polyvanadate (7.5 VO_x/nm²) monolayers (17).

X-ray diffraction measurements showed that VO_x species inhibit the conversion of metastable tetragonal ZrO₂ to its monoclinic form (Fig. 2a), as also reported for WO_x and other oxides supported on ZrO₂ (23–25). VO_x species also inhibit the crystallization of amorphous HfO₂ into monoclinic and orthorhombic structures (Fig. 2b), but they do not influence the crystallinity of the anatase TiO₂ structure

present in all VO_x/TiO₂ samples (Fig. 2e). Bulk V₂O₅ crystallites were not detected at any VO_x surface density within the experimental range on ZrO₂, HfO₂, or TiO₂ supports (Figs. 2a, 2b, 2e). Bulk V₂O₅ crystallites were also not detected on Al₂O₃- and SiO₂-supported samples with low VO_x surface density (<3 VO_x/nm²) (Figs. 2c, 2d). Higher surface densities on SiO₂ and Al₂O₃ lead to the appearance of V₂O₅ crystallites detectable by X-ray diffraction (Figs. 2c, 2d). X-ray line breadth analysis using the Scherrer equation shows that some of these crystallites on SiO₂ have diameters of 30–40 nm. Smaller V₂O₅ crystallites may also be present at lower VO_x densities on Al₂O₃ and SiO₂ and at all surface densities on ZrO₂, HfO₂, and TiO₂ supports, but they cannot be detected by diffraction methods because of their low concentration, poor crystallinity, or small numbers of unit cells. V₂O₅ crystallites detectable by X-ray diffraction appeared at lower VO_x surface densities on SiO₂ (3.5 VO_x/nm²) than on the other supports.

UV-visible absorption spectra reflect the electronic structure of valence bands in solids, but the broad nature of charge transfer features in the spectra of metal oxides makes it difficult to define the position of these bands from the energy at maximum absorption. Absorption edge energies provide a more convenient description of the electronic properties of solids. The absorption edge in all UV-visible spectra was determined using Tauc's law, an expression that describes the near-edge region in amorphous semiconductors and in crystalline semiconductors with indirect band gap transitions (26). Using this expression, the edge energy is obtained from the intercept of a straight line fitted through the rise of the function $[F(R_{\infty})/h\nu]^{1/2}$ plotted versus $h\nu$ (24), where $F(R_{\infty})$ is a Kubelka–Munk function (22), $h\nu$ is the energy of the incident photon. The position of the absorption edge for low-energy charge transfer transitions has been shown to correlate with the domain size of semiconductors and insulators (24, 27–35). The energy at the absorption edge has been recently used to characterize the size of MoO_x (33), WO_x (24), and VO_x (4, 35) domains in catalytic solids.

Typical diffuse reflectance UV-visible spectra are shown in Fig. 3 for VO_x/Al₂O₃ and VO_x/HfO₂ samples. Absorption bands in the 2–4 eV energy range reflect O²⁻ to V⁵⁺ ligand-to-metal charge transfer transitions (36–39). The corresponding charge transfer bands in Al₂O₃, SiO₂, HfO₂, and ZrO₂ occur at much higher energies and they do not interfere with the analysis of absorption edge regions corresponding to VO_x centers (Table 2). On TiO₂, however, this band appears at 3.17 eV and overlaps with the corresponding bands in VO_x species. In this case, VO_x electronic spectra were obtained by subtracting the TiO₂ bands from VO_x/TiO₂ spectra.

The effect of VO_x surface density on absorption edge energies is shown in Fig. 4 for the catalyst samples of this study. The absorption energy for bulk V₂O₅ (2.05 eV)

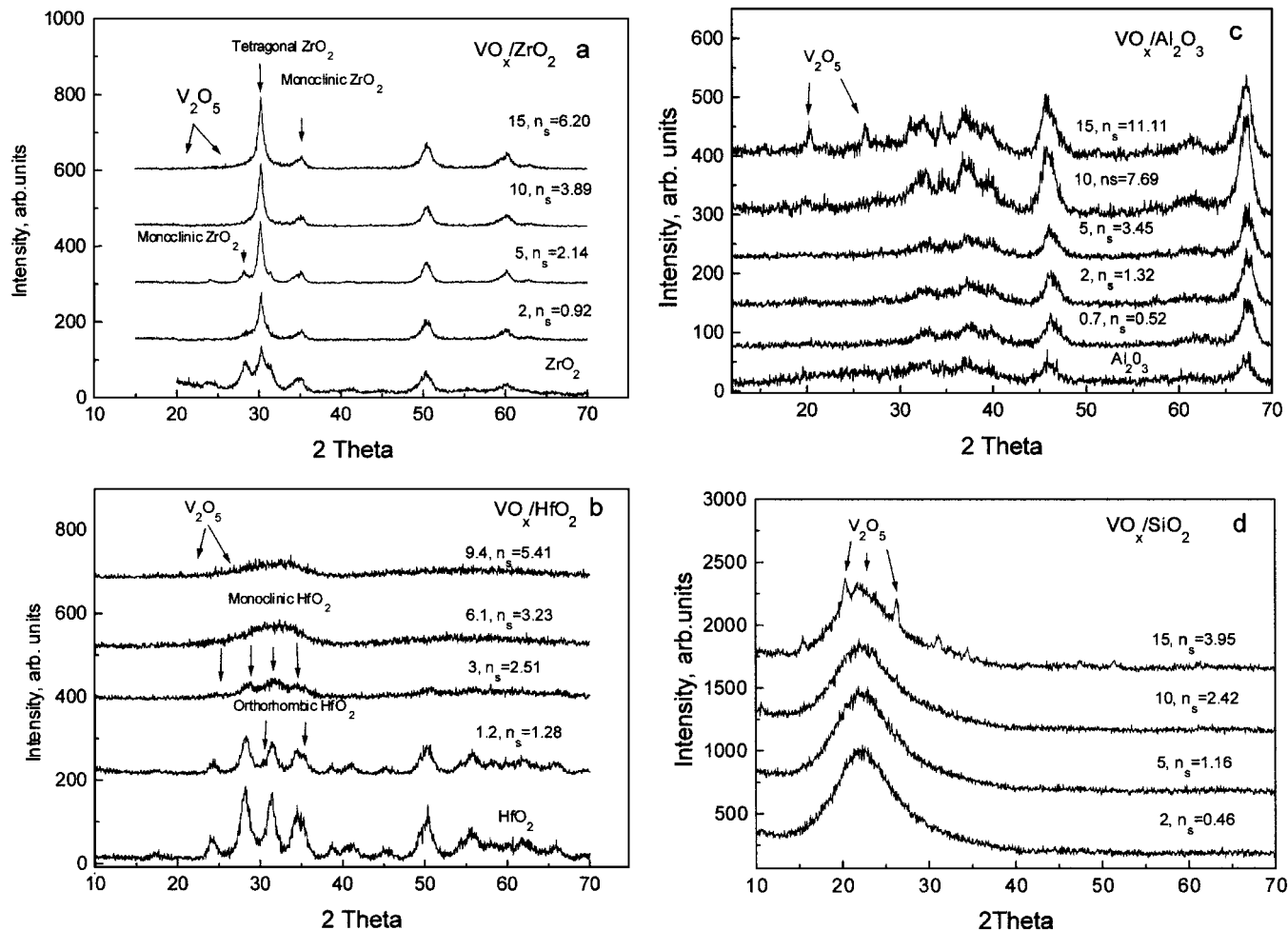


FIG. 2. X-ray diffraction patterns for VO_x/ZrO₂ (a); VO_x/HfO₂ (b); VO_x/Al₂O₃ (c); VO_x/SiO₂ (d); and VO_x/TiO₂ (e). {Legend (VO_x weight loading; n_s = VO_x surface density in VO_x/nm²)}.

calculated using Tauc's law is shown as a horizontal line in Fig. 4. The edge energy decreases with increasing VO_x surface density for all supports, as expected from an increase in the size and dimensionality of VO_x domains as VO_x surface density increases. At a given value of surface density, the identity of the support influences the apparent dispersion and absorption edge energy of VO_x species. Al₂O₃ and HfO₂ appear to disperse VO_x units more effectively than other supports and edge energies remain high (>2.5 eV), even at surface densities similar to those expected for polyvanadate monolayers (n_s = 7 VO_x/nm²). On silica supported catalysts, edge energies reach very low values (2.1 eV) at much lower surface densities (2–3 VO_x/nm²) than on other supports. The strength of interactions between VO_x and ZrO₂ or TiO₂ supports appears to lie between the extremes observed on Al₂O₃ and SiO₂ supports (Fig. 4), because absorption energies lie between those measured on VO_x/Al₂O₃ and VO_x/SiO₂ supports.

TABLE 2
UV-Visible Absorption Edge in Standard Bulk Compounds

Compound	UV-visible absorption edge (eV)	Number of vanadium polyhedrons in the first coordination shell	Reference
V ₂ O ₅	2.05 ^a	5	This work
OV[OSiO(t-Bu) ₃] ₃	3.65 ^a	0	(54)
ZrO ₂	5.0	—	(55)
HfO ₂	5.6	—	(55)
TiO ₂	3.2	—	(56)
SiO ₂	10.4	—	(57)
Al ₂ O ₃	8.7	—	(58)

^a UV-vis absorption edge energies were calculated using Tauc's law for indirect and amorphous semiconductors (26).

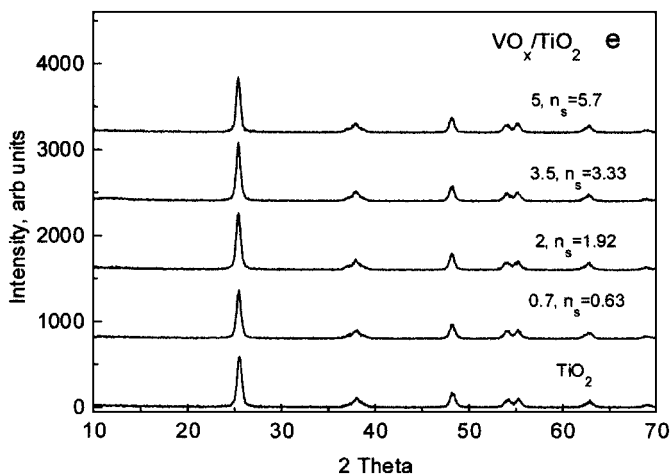


FIG. 2—Continued

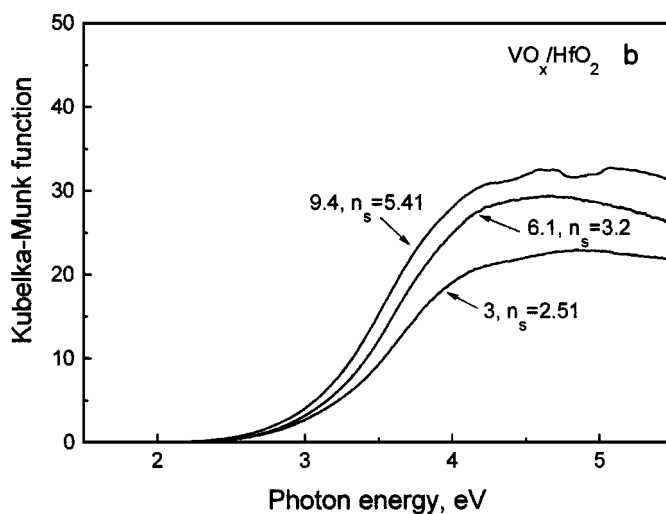
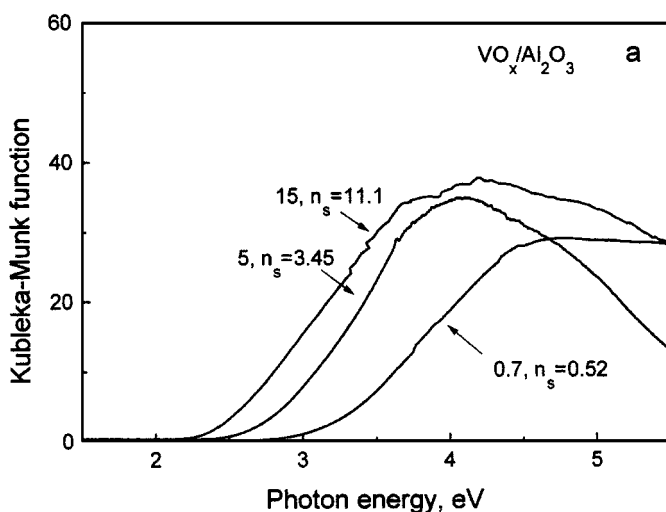


FIG. 3. UV-visible spectra for VO_x/Al₂O₃ catalysts {Legend (VO_x weight loading; n_s = VO_x surface density in VO_x/nm²)}.

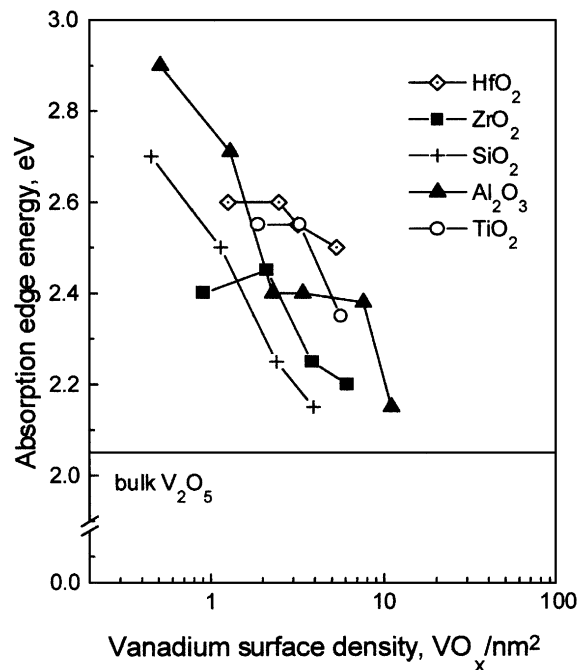


FIG. 4. Effect of VO_x surface density on absorption edge energies for supported vanadium oxide catalysts.

Raman spectra for catalysts with VO_x surface densities of 3.9–7.7 VO_x/nm² and 2.1–3.3 VO_x/nm² are shown in Figs. 5a and 5b, respectively. The positions of the bands associated with various VO_x species are listed in Table 3. The narrow band at 1030–1020 cm⁻¹ is assigned to V=O stretching modes within isolated monovanadate species. The broad bands in the 1000–600 cm⁻¹ region can be ascribed to V=O (1000–800 cm⁻¹) and V-O-V (800–600 cm⁻¹) stretching modes in polyvanadate species (18, 40, 41). Bulk V₂O₅ can be identified by bands at about 143, 282, 405, 489, 524, 694, and 993 cm⁻¹, very similar to those detected on the V₂O₅/SiO₂ samples shown in Table 3. It is notable that Raman spectroscopy provides evidence for V₂O₅ crystallites at much lower VO_x surface densities on all of the supports than does XRD, indicating greater sensitivity of Raman spectroscopy to the presence of crystalline V₂O₅.

The structure of the VO_x species detected by Raman spectroscopy depends on both support composition and VO_x surface density. In VO_x/SiO₂, the only bands detected are those for monovanadate species and V₂O₅. As the VO_x surface density increases from 2.4 to 4.0 VO_x/nm², the proportion of V₂O₅ to monovanadate species increases. On Al₂O₃, no features are observed above the background when the surface density is 2.3 VO_x/nm². At higher surface densities (7.7 VO_x/nm²), peaks attributed to monovanadate species and V₂O₅ are detected. For vanadia supported on TiO₂, HfO₂, and ZrO₂, the most intense Raman bands correspond to monovanadate and polyvanadate species. The maximum intensity for the broad polyvanadate bands

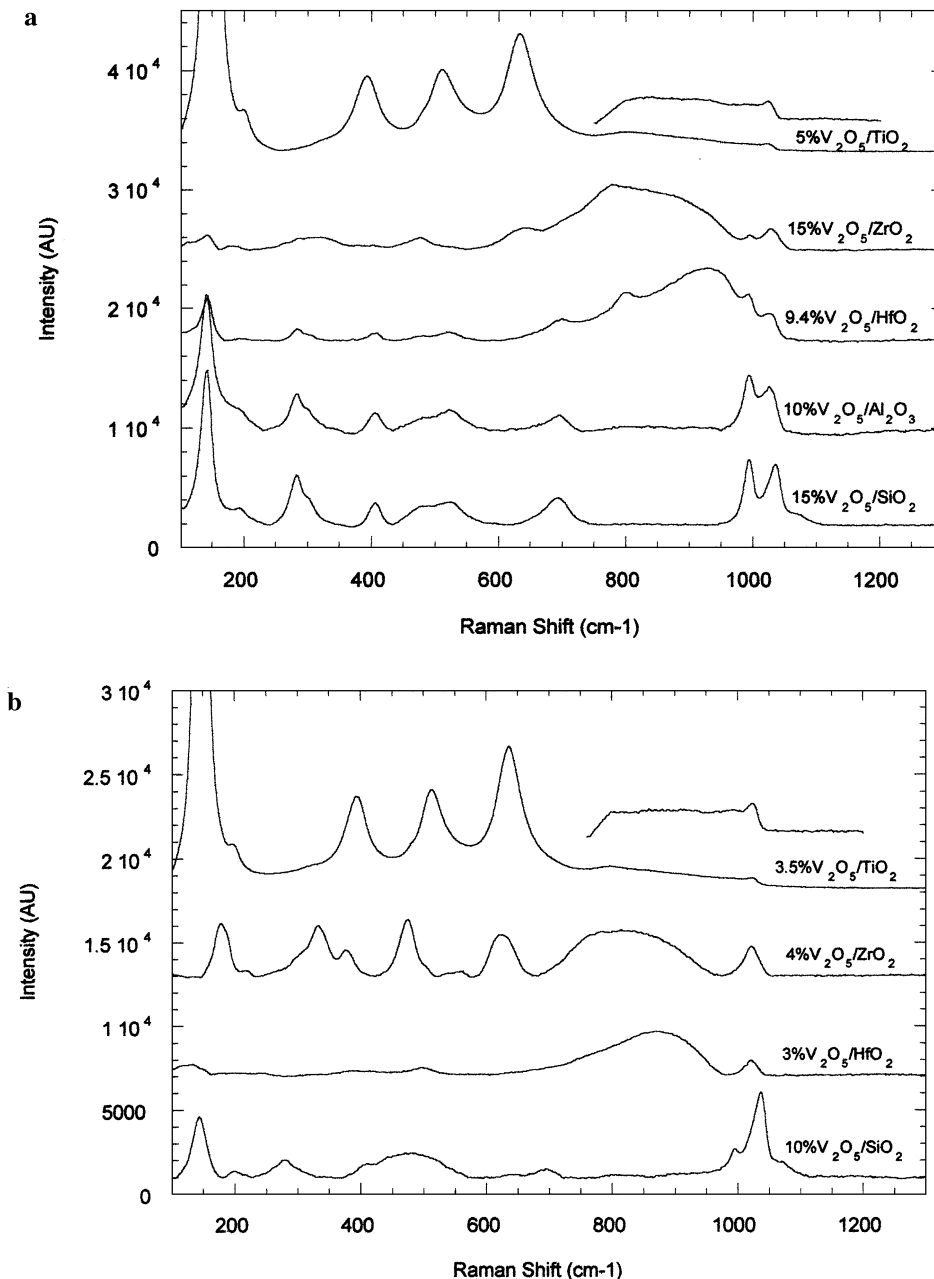


FIG. 5. Raman spectra of supported vanadium oxide catalysts with VO_x surface densities of (a) $3.9\text{--}7.7 \text{ VO}_x/\text{nm}^2$ and (b) $2.1\text{--}3.3 \text{ VO}_x/\text{nm}^2$ [Legend (VO_x weight loading; $n_s = \text{VO}_x$ surface density in VO_x/nm^2)].

($1000\text{--}600 \text{ cm}^{-1}$) shifts to lower frequencies as the support changes from HfO_2 to ZrO_2 to TiO_2 , suggestive of an increasing percentage of V-O-V species relative to V=O bonds. Figure 5a shows that at higher VO_x surface densities, weak bands corresponding to support-vanadia compounds are detected on HfO_2 and ZrO_2 . These bands are located at 772 and 977 cm^{-1} (Fig. 5a), in agreement with Raman spectra reported for bulk ZrV_2O_7 (40, 42).

The catalytic properties of all supported vanadium oxide samples are reported in Figs. 6–8. The effect of bed resi-

dence time on C_3H_8 conversion and on C_3H_6 , CO, and CO_2 selectivities is shown for $\text{VO}_x/\text{Al}_2\text{O}_3$ ($n_s = 3.5 \text{ VO}_x/\text{nm}^2$) and VO_x/HfO_2 ($n_s = 3.2 \text{ VO}_x/\text{nm}^2$) in Figs. 6a and 6b, respectively. CO_x selectivities increase with increasing bed residence time, suggesting that C_3H_6 undergoes secondary oxidation reactions to form CO_x . Selectivities extrapolated to zero residence time reflect the relative rates of direct conversion of C_3H_8 to C_3H_6 and to CO_x .

Figure 7 shows propane reaction rates normalized by the number of V-atoms and extrapolated to zero conversion

TABLE 3
Raman Band Assignments for Vanadium Oxide Species (A) High VO_x Surface Density Samples;
(b) Low VO_x Surface Density Samples

Sample (VO _x /nm ²)	Monovanadate (V=O)	Polyvanadate (V=O & V-O-V)	V ₂ O ₅	Support (phase)
<i>A. Raman peaks for high surface density samples</i>				
15% V ₂ O ₅ /SiO ₂ (3.95)	1035	None	143, 282, 406, 489, 524, 694, 993	
10% V ₂ O ₅ /Al ₂ O ₃ (7.69)	1025	None	140, 282, 406, 495, 521, 696, 993	
5% V ₂ O ₅ /TiO ₂ (5.70)	1022	750–950 (810)	None	~150, 393, 511, 633 (anatase)
15% V ₂ O ₅ /ZrO ₂ (6.20)	1028	700–980 (778) ^a	143, 995	313, 477, 640 (tetragonal)
9.4% V ₂ O ₅ /HfO ₂ (5.41)	1027	820–980 (939), 803 ^b	143, 282, 408, 489, 524, 993	702 (?)
<i>B. Raman peaks for low surface density samples</i>				
10% V ₂ O ₅ /SiO ₂ (2.42)	1036	None	143, 280, 486, 695, 995	
3.5% V ₂ O ₅ /TiO ₂ (3.33)	1022	750–950 (810)	None	148, 395, 513, 636 (anatase)
4% V ₂ O ₅ /ZrO ₂ (2.14)	1022	690–970 (780)	None	330, 475, 626 (tetragonal) 178, 377, 562 (monoclinic(?))
3% V ₂ O ₅ /HfO ₂ (2.51)	1021	750–980 (880)	None	500 (?)

^a ZrV₂O₇.

^b HfV₂O₇.

as a function of VO_x surface density for all catalysts. In general, oxidative dehydrogenation rates increase with increasing VO_x surface density. No reaction products were detected on pure ZrO₂, HfO₂, SiO₂, and Al₂O₃ supports at our reaction conditions. On pure TiO₂, however, propane reaction rates were significant (2.2×10^{-7} mol/g-s) and initial C₃H₆ selectivities were low (42%). The support activity was subtracted by assuming that the surface of VO_x/TiO₂ consisted of bare patches with reaction rates characteristic of pure TiO₂ and that the rest of the surface was covered with polyvanadate domains. Oxidative dehydrogenation rates per V-atom were highest on VO_x/ZrO₂ (Fig. 7). On HfO₂, TiO₂, and Al₂O₃ supports, reaction rates (per V-atom) increased with increasing VO_x density and approached the higher rates observed on ZrO₂ as surface densities increased above 5 VO_x/nm². Reaction rates were very low on SiO₂-supported catalysts, probably due to the presence of inactive monovanadate species and to the low V₂O₅ dispersion detected by X-ray diffraction, UV-visible, and Raman measurements.

Figure 8 shows that C₃H₆ selectivities extrapolated to zero oxygen conversion increase with increasing VO_x surface density for all catalysts (Fig. 8). Selectivities were

corrected for reactions on TiO₂ for VO_x/TiO₂ catalysts. Propene selectivities are similar (70–90%) on all catalysts at a given value of VO_x surface density, except for slightly higher values on Al₂O₃-supported catalysts at surface densities below 10 VO_x/nm². It appears that the larger VO_x domains expected at higher surface densities favor oxidative dehydrogenation over competing pathways leading to the direct oxidation of propane to CO and CO₂.

DISCUSSION

X-ray diffraction and UV-visible and Raman spectroscopy data show that the structure of dispersed VO_x species depends on the identity of the support and on VO_x surface density (*n_s*). Vanadia dispersed on Al₂O₃ shows the broadest range of VO_x structures among the materials examined in this study. At VO_x surface densities below 1 VO_x/nm², the large absorption edge energies in UV-visible spectra and the absence of polyvanadate bands in Raman spectra suggest that VO_x species exist as monovanadate structures or as isolated V⁺⁵ centers occupying cation vacancies within the Al₂O₃ lattice (43). For surface densities between 1 and

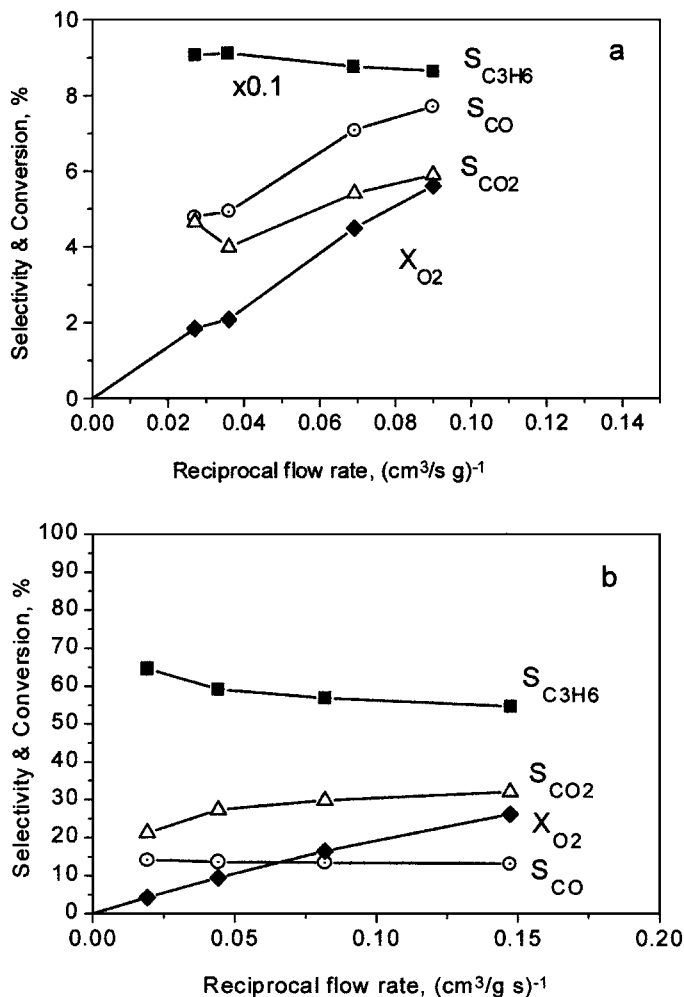


FIG. 6. Product selectivities and oxygen conversions in oxidative dehydrogenation of propane on (a) 5 VO_x/Al₂O₃ ($n_s = 3.5$ VO_x/nm²) and (b) 6.1 VO_x/HfO₂ ($n_s = 3.2$ VO_x/nm²). Reaction conditions: 606 K, 14.03 kPa C₃H₈, 1.74 kPa O₂.

7 VO_x/nm², UV-visible and Raman spectra detect the co-existence of polyvanadate and monovanadate species on Al₂O₃. Above 7 VO_x/nm², small V₂O₅ crystallites become visible by X-ray diffraction and Raman bands corresponding to crystalline V₂O₅ appear in the spectrum (Fig. 5a, Table 3).

The structural evolution of dispersed VO_x species on HfO₂, TiO₂, and ZrO₂ is very similar to that observed on Al₂O₃. UV-visible and Raman spectra show that polyvanadate and monovanadate species co-exist on these support surfaces at VO_x surface densities above 1 VO_x/nm². Crystalline V₂O₅ species were not detected on any of the supports at surface densities below about 5 VO_x/nm². Higher oxidation temperatures lead to the formation of V₂O₅ clusters and of zirconium vanadate on ZrO₂ at surface densities above 10 VO_x/nm² (4, 42, 44). Isolated tetrahedral monovanadate species have also been detected using

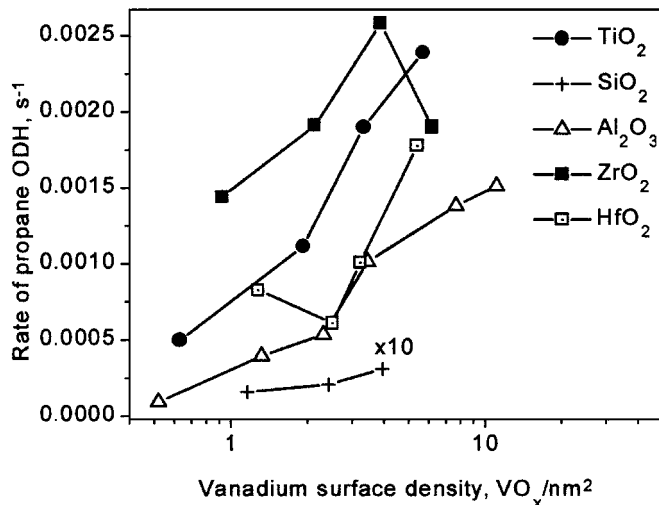


FIG. 7. Effect of VO_x surface density on oxidative dehydrogenation rates (per V-atom) on supported vanadium oxide catalysts. Reaction conditions: 606 K, 14.03 kPa C₃H₈, 1.74 kPa O₂.

⁵¹V NMR and X-ray absorption spectroscopy at very low vanadium surface densities on Al₂O₃ and other supports (45, 46).

On SiO₂-supported samples, X-ray diffraction and Raman spectroscopy do not detect V₂O₅ crystallites at surface densities of about 1 VO_x/nm². Both techniques clearly show the presence of crystalline V₂O₅ at higher surface densities (>4 VO_x/nm²). V₂O₅ crystallites become detectable by X-ray diffraction on SiO₂ at lower surface densities (4.0 VO_x/nm²) than on the other supports. VO_x species interact weakly with SiO₂ and form V₂O₅ clusters well below surface densities required to complete a polyvanadate monolayer (7.5 VO_x/nm²) (Fig. 2). Previous

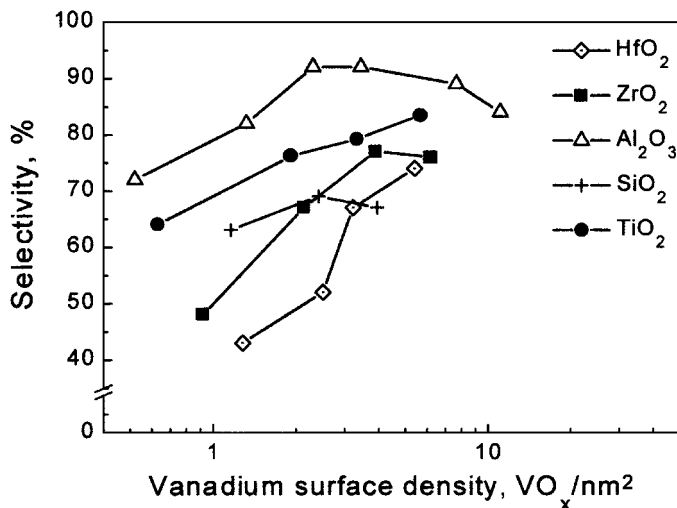


FIG. 8. Effect of VO_x surface density on initial (primary) propene selectivities on supported vanadium oxide catalysts. Reaction conditions: 606 K, 14.03 kPa C₃H₈, 1.74 kPa O₂.

studies have also shown that VO_x dispersion is lower on SiO_2 than on Al_2O_3 or TiO_2 for a given vanadium content (47).

UV-visible spectra confirm the conclusions reached from Raman and X-ray diffraction studies. For example, edge energies for 10 VO_x/SiO_2 and 15 VO_x/SiO_2 were lower (2.1–2.2 eV) than for other supports with the same vanadium surface densities ($n_s = 2.4\text{--}4.0 \text{ VO}_x/\text{nm}^2$) (Fig. 4), suggesting larger VO_x domains on SiO_2 than on the other supports. At lower vanadium surface densities, the higher energy of UV-Vis absorption edge suggests the presence of isolated monovanadate species on this support. The high absorption energies on HfO_2 and Al_2O_3 at low VO_x surface densities ($<4 \text{ VO}_x/\text{nm}^2$) suggest the predominant presence of monovanadate species (Fig. 4). Polyvanadate domains or small V_2O_5 clusters account for the intermediate absorption energies observed on ZrO_2 (Fig. 4). Absorption edge energies decreased with increasing VO_x surface densities on all supports, as expected from the growth of VO_x domains as VO_x surface density increases. Absorption edge energies decrease with increasing number of next nearest neighbors for MoO_x (33) and WO_x (24). Similar effects were observed for VO_x species in standard compounds (Table 2). These shifts reflect mainly the delocalization of molecular orbitals over larger domains and they appear to be influenced only weakly by changes in local coordination (48).

Oxidative dehydrogenation rates (per V-atom) on supported vanadia depend on support composition and on VO_x surface density (Fig. 7). In general, reaction rates (per V-atom) increase as VO_x surface density increases for all supports, suggesting that polyvanadate domains are more active than monovanadate species. The data in Fig. 7 show that ZrO_2 -supported catalysts show the highest oxidative dehydrogenation rates and SiO_2 -supported catalysts the lowest activity, while the other supports give intermediate reactions rates ($\text{TiO}_2 > \text{HfO}_2 > \text{Al}_2\text{O}_3$). On Al_2O_3 , monovanadate structures favored at low surface densities show high propene selectivities, but very low reaction rates (Fig. 7). Reaction rates increase markedly as the coverage of polyvanadate structures and the UV-visible edge energies increase with increasing VO_x surface density on Al_2O_3 . Monovanadate structures present on Al_2O_3 at low VO_x surface densities are not very active, apparently because oxidative dehydrogenation turnovers require reduction-oxidation cycles of V^{+5} centers and V-O-Al species appear to be more difficult to reduce than V-O-V or V=O sites in polyvanadate species. This conclusion is consistent with reducibility studies using H_2 as the reductant (49).

The very low apparent ODH turnover rates on VO_x/SiO_2 reflect the co-existence of inactive isolated monovanadate species and active but poorly dispersed bulk V_2O_5 , as shown by the Raman spectra of VO_x/SiO_2 . The observed ODH rates are caused by the poor dispersion of the V_2O_5 crystallites. The ODH turnover rate estimated

for bulk V_2O_5 based on its BET surface area and a surface density of 7 VO_x/nm^2 is $2.25 \times 10^{-3} \text{ s}^{-1}$ at the conditions of our experiments. True turnover rates may be actually higher because not all low-index planes in V_2O_5 expose V=O and V-O-V structures. The apparent turnover rates on VO_x/SiO_2 samples are much lower than these values ($2\text{--}3 \times 10^{-5} \text{ s}^{-1}$, Fig. 7). These data suggest that the fraction of VO_x sites available at the surface of V_2O_5 crystallites supported on SiO_2 is about 0.01. This value is consistent with the large crystallites (30–40 nm) detected by line breadth analysis of X-ray diffraction lines for VO_x/SiO_2 samples.

The observed effects of support and VO_x surface density on reaction rates can be best interpreted by examining the dependence of oxidative dehydrogenation rates on VO_x domain size, as given indirectly by UV-visible edge energies in Fig. 9. Reaction rates (per total V-atom) increase monotonically as absorption edge energies decrease from 2.9 to 2.2 eV (Fig. 9). These rates reach maximum values of $2.0\text{--}2.5 \times 10^{-3} \text{ s}^{-1}$ at absorption energies of about 2.2 eV. This trend clearly shows that polyvanadate domains contain surface sites with higher activity than those present on isolated monovanadate species, which have UV-Vis absorption edges at about 3.65 eV (Table 2). Reaction rates normalized by the surface area and the VO_x surface density of V_2O_5 are similar to those obtained on the most active supported catalysts, suggesting that polyvanadate domains attain surface structures with catalytic properties resembling those of bulk V_2O_5 . As discussed above, the unusually low activity of VO_x/SiO_2 reflects the presence of inactive monovanadate species and the low dispersion of V_2O_5 crystallites on this support.

Clearly, the VO_x surface density required for densification of VO_x structures into polyvanadates and V_2O_5 clusters depends on the identity of the support. The observed

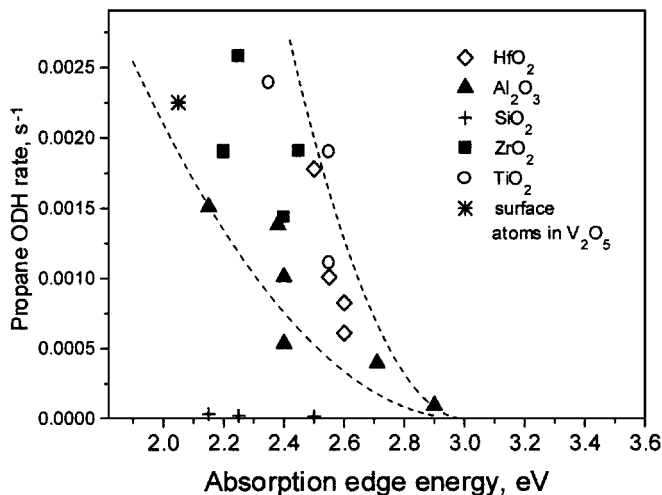
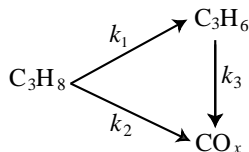


FIG. 9. Dependence of propane oxidative dehydrogenation rates (per V-atom) on the absorption edge energy. Reaction conditions: 606 K, 14.03 kPa C_3H_8 , 1.74 kPa O_2 .

catalytic trends, however, become less dependent on the support when the VO_x domain size or dispersion is characterized by UV-visible edge energies (Fig. 9). Polyvanadates with high turnover rates and accessibility form domains of size and structure controlled by the strength of VO_x -support interactions. Once formed, however, the reaction rates and electronic properties of these VO_x domains (reflected in their absorption edge energies) becomes much more weakly dependent on the identity of the support.

Bridging V-O-V groups in two-dimensional VO_4 arrays, which are favored at high vanadium coverages, have been proposed as active sites for oxidative dehydrogenation on $\text{VO}_x/\text{Al}_2\text{O}_3$ (50). Ethane reaction rates (per V-atom) and ethene selectivity increase with increasing vanadium loading on SiO_2 supports (51). Turnover rates (calculated from site density measurements using O_2 chemisorption uptakes after reaction) also increased with increasing V-loading (51). In the same study, V=O species were proposed as active dehydrogenation sites and V-O-Si structures were considered to provide combustion sites. On Nb_2O_5 - V_2O_5 catalysts, turnover rates per surface V-atom increased with VO_x surface coverage, measured by surface-sensitive ion scattering techniques (52). The higher turnover rates and selectivity on polyvanadate and V_2O_5 structures is well documented, but molecular sieves containing V-atoms in presumed isolation are also active in oxidative dehydrogenation reactions (3, 5, 12). This has led to the conclusion that vanadate monomers, dimers, and polymers can all provide active and selective sites for alkane oxidative dehydrogenation (1). Our study provides strong evidence, however, that monovanadate structures are significantly less active than polyvanadates for oxidative dehydrogenation of propane.

Residence time effects on product selectivity (Fig. 6) show that C_3H_8 - O_2 mixtures react in parallel and sequential steps, as shown also in previous studies (1–3):



Pseudo-first-order rate coefficients for dehydrogenation (k_1) and combustion (k_2) pathways and for secondary combustion of propene (k_3) can be obtained from bed residence time data. The assumption that all steps are first order in hydrocarbon is consistent with our kinetic data on VO_x/ZrO_2 catalysts. The oxygen order implicit in the pseudo-first-order rate coefficients is not required in the kinetic analysis because oxygen conversions were very low (<2%). The details of the kinetic analysis have been reported elsewhere (4).

The measured values of k_1 increase with increasing VO_x surface density, in agreement with similar trends shown in Fig. 7 for initial oxidative dehydrogenation rates. The

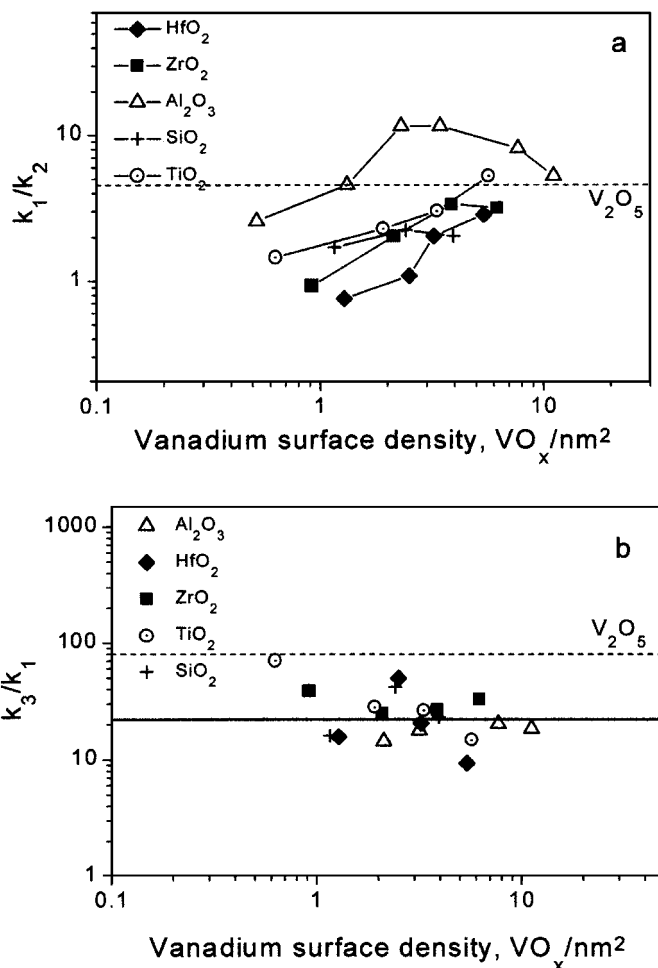


FIG. 10. Dependence of (a) k_1/k_2 and (b) k_3/k_1 rate constant ratios on VO_x surface density for supported vanadium oxide catalysts. Reaction conditions: 606 K, 14.03 kPa C_3H_8 , 1.74 kPa O_2 .

effects of VO_x surface density on k_1/k_2 and k_3/k_1 ratios are shown in Figs. 10a and 10b, respectively. For surface densities between 1 and $8 \text{ VO}_x/\text{nm}^2$, k_1/k_2 ratios increase with surface density, indicating that primary dehydrogenation is favored over primary combustion on larger polyvanadate domains. Except for Al_2O_3 , all supports show similar k_1/k_2 values at a given VO_x surface density. The high k_1/k_2 values of Al_2O_3 reflect lower values for k_2 on this support, since k_1 values on these samples are comparable to those measured on the other supports. It appears that primary propane oxidation is inhibited as VO_x species titrate unselective sites on support surfaces and as less active monovanadate structures are replaced by more active polyvanadate domains. The similarity between the k_1/k_2 ratio for bulk V_2O_5 powders (4.5) and for supported samples with high VO_x surface densities (2–5 VO_x/nm^2) shows that the relative rates of primary dehydrogenation and combustion steps are essentially the same for catalysis on polyvanadates, small VO_x clusters, and bulk V_2O_5 powders. Intraparticle diffusional restrictions

can corrupt the kinetic nature of these k_1/k_2 ratios by causing propene combustion reactions within diffusion-limited particles to appear to be propane combustion steps. The observed increase in k_1/k_2 ratios as VO_x surface density increases (Fig. 10a) rules out this possibility, because such diffusional restrictions would become more severe and lead to lower k_1/k_2 ratios as the catalyst volumetric productivity increases with increasing VO_x site density (53).

The measured k_3/k_1 values, however, do not vary systematically with support composition or VO_x surface density (Fig. 10b). The range of k_3/k_1 values (10–60) in these samples is similar to those measured on VO_x/ZrO_2 catalysts with a wider range of VO_x surface densities (4). The values obtained on bulk V_2O_5 powders (Fig. 10b) lie at the upper end of this range. It appears that propane dehydrogenation and propene combustion rate coefficients vary similarly with VO_x structure and domain size, suggesting that similar surface structures are required for these two reactions. Combustion rate coefficients (k_3), however, are much higher than those for oxidative dehydrogenation (k_1) at the reaction conditions of this study. The similar structural requirements, satisfied by polyvanadates or V_2O_5 surfaces, and the higher rates of secondary reactions lead to low propene yields on vanadia catalysts. If primary dehydrogenation and secondary combustion indeed share common structural requirements, it appears unlikely that structural modifications of V-centers beyond those attained by changes in domain size can overcome current propene yield limits. Cyclic dehydrogenation/reoxidation and membrane reactor schemes may provide a more effective strategy for increasing propene yields above those currently accessible in steady-state operation of supported vanadium oxide catalysts.

CONCLUSIONS

The structure and dispersion of VO_x species depend on their surface density and on their interaction with a given support. Support surfaces predominantly covered with polyvanadate structures or small V_2O_5 clusters containing V-O-V or V=O linkages lead to high oxidative dehydrogenation rates and selectivities. The composition of the support influences the speciation of VO_x species into monovanadates, polyvanadates, and V_2O_5 clusters and thus the catalytic behavior of supported vanadia in oxidative dehydrogenation reactions. The concentration of polyvanadate structures increases with increasing VO_x surface density. Raman and UV-visible spectra show an excellent correlation between oxidative dehydrogenation rates and the density of polyvanadate species on all support surfaces. Oxidative dehydrogenation rate coefficients increase initially with increasing VO_x surface density on all supports, concurrently with the densification of isolated monovanadates into polyvanadate domains, but ultimately decrease as the

latter evolve into V_2O_5 crystallites with low specific surface area. Ratios of rate coefficients for oxidative dehydrogenation of propane to those for secondary propene combustion are relatively insensitive to structural modifications caused by changes in VO_x surface density or support composition. This suggests that sites required for oxidative dehydrogenation also catalyze the undesired combustion of propene.

ACKNOWLEDGMENTS

This work was supported by the Director, Office of Basic Energy Sciences, Chemical Sciences Division, of the U.S. Department of Energy under Contract DE-AC03-76SF00098.

REFERENCES

- Blasko, T., and López Nieto, J. M., *Appl. Catal. A* **157**, 117 (1997).
- Kung, H. H., *Adv. Catal.* **40**, 1 (1994).
- Albonetti, S., Cavani, F., and Trifiro, F., *Catal. Rev.-Sci. Eng.* **38**, 413 (1996).
- Khodakov, A., Yang, J., Su, S., Iglesia, E., and Bell, A. T., *J. Catal.* **177**, 343 (1998).
- Centi, G., and Trifiro, F., *Appl. Catal. A* **143**, 3 (1996).
- Mamedov, E. A., and Cortés-Corberan, V., *Appl. Catal. A* **127**, 1 (1995).
- Busca, G., *Catal. Today* **24**, 307 (1995).
- Michalakos, P., Kung, M. C., Jahan, I., and Kung, H. H., *J. Catal.* **140**, 226 (1993).
- Owens, L., and Kung, H. H., *J. Catal.* **148**, 587 (1994).
- Corma, A., López Nieto, J. M., and Paredes, N., *J. Catal.* **144**, 425 (1993).
- Sananes-Schulz, M. T., Tuel, A., Hutchings, G. J., and Volta, J. C., *J. Catal.* **166**, 388 (1997).
- Zatorski, L. W., Centi, G., López Nieto, J. M., Trifiro, F., Belussi, G., and Fattore, V., *Stud. Surf. Sci. Catal.* **49**, 1243 (1989).
- Gao, X., Ruiz, P., Xin, Q., Guo, X., and Delmon, B., *J. Catal.* **148**, 56 (1995).
- Corma, A., López Nieto, J. M., Paredes, N., Pérez, M., Shen, Y., Cao, H., and Suib, S. L., *Stud. Surf. Sci. Catal.* **72**, 213 (1992).
- Hanuza, J., Jezowska-Trzebiatowska, B., and Oganowski, W., *J. Mol. Catal.* **29**, 109 (1985).
- Blasko, T., Concepción, P., López Nieto, J. M., and Pérez-Pariente, J., *J. Catal.* **152**, 1 (1995).
- Centi, G., *Appl. Catal. A* **147**, 267 (1996).
- Wachs, I. E., and Weckhuysen, B. M., *Appl. Catal. A* **157**, 67 (1997).
- Schart, U., Schrami-Marth, M., Wokaun, A., and Baiker, J., *J. Chem. Soc., Faraday Trans.* **87**, 3299 (1991).
- Deo, G., and Wachs, I. E., *J. Phys. Chem.* **95**, 5889 (1991).
- Oyama, S. T., Went, G. T., Lewis, K. B., Bell, A. T., and Somorjai, G. A., *J. Phys. Chem.* **93**, 6786 (1989).
- Delgass, W. N., "Spectroscopy in Heterogeneous Catalysis." Academic Press, New York, 1979.
- Mercera, P. D. L., van Ommen, J. G., Desburg, E. B. M., Burggraaf, A. J., and Ross, J. R. H., *Appl. Catal.* **71**, 363 (1991).
- Barton, D. G., Shtein, M., Wilson, R. D., Soled, S. L., and Iglesia, E., *J. Phys. Chem.*, submitted. [Iglesia, E., Barton, D. G., Soled, S. L., Miso, S., Baumgartner, J. E., Gates, W. E., Fuentes, G. A., and Meitzner, G. D., *Stud. Surf. Sci. Catal.* **101**, 533 (1996)]
- Zhao, B.-Y., Xu, X.-P., Ma, H.-R., Sun, D.-H., and Gao, J.-M., *Catal. Lett.* **45**, 237 (1997).
- Tauc, J., in "Amorphous and Liquid Semiconductors" (J. Tauc, Ed.). Plenum, London, 1974.

27. Cherstnoy, N., Hull, R., and Brus, L. E., *J. Chem. Phys.* **85**, 2237 (1986).
28. Alivisatos, A. P., *Science* **271**, 933 (1996).
29. Service, R. F., *Science* **271**, 920 (1996).
30. Hoener, C. F., Allan, K. A., Bard, A. J., Campion, A., Fox, M. A., Mallouk, T. E., Webber, S. E., and White, J. M., *J. Phys. Chem.* **96**, 3812 (1992).
31. Liu, Z., and Davis, R. J., *J. Phys. Chem.* **90**, 2555 (1986).
32. Wang, Y., Mahler, S. W., and Kasowski, R., *J. Chem. Phys.* **87**, 7315 (1987).
33. Weber, R. S., *J. Catal.* **151**, 470 (1995).
34. Fournier, M., Louis, C., Che, M., Chaquin, P., and Masure, P., *J. Catal.* **119**, 400 (1989).
35. Wei, D., and Haller, G. L., in "Proceedings 2nd Memorial G. K. Borekov Intern. Conference, Novosibirsk, July, 1997," p. 110.
36. Good, M. L., *Spectrochim. Acta A* **29**, 707 (1973).
37. So, H., and Pope, M. T., *Inorg. Chem.* **11**, 1441 (1972).
38. Iwamoto, M., Furukawa, H., Matsukami, K., Takenaka, T., and Kagawa, S., *J. Amer. Chem. Soc.* **105**, 3719 (1983).
39. Ronde, H., and Snijders, J. G., *Chem. Phys. Lett.* **50**, 282 (1977).
40. Roozeboom, F., Mittelmeijer-Hazelger, M. C., Moulijn, J. A., de Beer, J., and Gellings, P. J., *J. Phys. Chem.* **84**, 2783 (1980).
41. Wachs, I. E., *Catal. Today* **27**, 437 (1996).
42. Sanati, M., Andersson, A., Wallenberg, L. R., and Rebenstorf, B., *Appl. Catal. A* **106**, 51 (1993).
43. El-Shobaky, G. A., El-Nabarawy, T., Fagal, G. A., and Mokhtar, M., *J. Thermal Anal.* **46**, 1473 (1996).
44. Sohn, J. R., Gho, S. G., Pae, Y. I., and Hayashi, S., *J. Catal.* **159**, 170 (1996).
45. Eckert, H., and Wachs, I. E., *J. Phys. Chem.* **93**, 6796 (1989).
46. Inumaru, K., Misono, M., and Okuhara, T., *Appl. Catal. A: General* **149**, 133 (1997).
47. Went, G. T., Oyama, S. T., and Bell, A. T., *J. Phys. Chem.* **94**, 4240 (1990).
48. Masure, D., Chaquin, P., Louis, C., Che, M., and Fournier, M., *J. Catal.* **119**, 415 (1989).
49. Khodakov, A., Bell, A. T., and Iglesia, E., unpublished results.
50. Eon, J. G., Olier, R., and Volta, J. C., *J. Catal.* **145**, 318 (1994).
51. Oyama, S. T., *J. Catal.* **128**, 210 (1991).
52. Smits, R. H. H., Seshan, K., Ross, J. R. H., van den Oetelaar, L. C. A., Helweggen, J. H., Anantharaman, M. R., and Brongersma, H. H., *J. Catal.* **157**, 584 (1995).
53. Koros, R. M., and Nowak, E. J., *Chem. Eng. Sci.* **22**, 470 (1967).
54. Rulkens, R., private communication.
55. Bendoraitis, J. G., and Salomon, R. E., *J. Phys. Chem.* **69**, 3666 (1965).
56. Anpo, M., Shima, T., Kodama, S., and Kubokawa, Y., *J. Phys. Chem.* **91**, 4305 (1987).
57. Klein, G., and Chun, H. O., *Phys. Status Solidi B* **49**, 167 (1972).
58. Ealet, B., Elyakhloufu, M. H., Gillet, E., and Ricci, M., *Thin Solid Films* **250**, 92 (1994).